Monthly Notices
of the
ROYAL ASTRONOMICAL SOCIETY

Mon. Not. R. Astron. Soc. **401,** 1564–1569 (2010) doi:10.1111/j.1365-2966.2009.15789.x

Swift/XRT monitoring of the supergiant fast X-ray transient IGR J18483−0311 for an entire orbital period

P. Romano,[1⋆] L. Sidoli,[2] L. Ducci,[2,3] G. Cusumano,[1] V. La Parola,[1] C. Pagani,[4] K. L. Page,[5] J. A. Kennea,[4] D. N. Burrows,[4] N. Gehrels,[6] V. Sguera[7] and A. Bazzano[7]

[1]*INAF, Istituto di Astrofisica Spaziale e Fisica Cosmica, Via U. La Malfa 153, I-90146 Palermo, Italy*
[2]*INAF, Istituto di Astrofisica Spaziale e Fisica Cosmica, Via E. Bassini 15, I-20133 Milano, Italy*
[3]*Dipartimento di Fisica e Matematica, Università dell'Insubria, Via Valleggio 11, I-22100 Como, Italy*
[4]*Department of Astronomy and Astrophysics, Pennsylvania State University, University Park, PA 16802, USA*
[5]*Department of Physics & Astronomy, University of Leicester, LE1 7RH*
[6]*NASA/Goddard Space Flight Center, Greenbelt, MD 20771, USA*
[7]*INAF, Istituto di Astrofisica Spaziale e Fisica Cosmica, Via Fosso del Cavaliere 100, I-00133, Roma, Italy*

Accepted 2009 September 25. Received 2009 September 23; in original form 2009 July 23

ABSTRACT

IGR J18483−0311 is an X-ray pulsar with transient X-ray activity, belonging to the new class of high-mass X-ray binaries called supergiant fast X-ray transients. This system is one of the two members of this class, together with IGR J11215−5952, where both the orbital (18.52 d) and spin period (21 s) are known. We report on the first complete monitoring of the X-ray activity along an entire orbital period of a supergiant fast X-ray transient. These *Swift* observations, lasting 28 d, cover more than one entire orbital phase consecutively. They are a unique data set, which allows us to constrain the different mechanisms proposed to explain the nature of this new class of X-ray transients. We applied the new clumpy wind model for blue supergiants developed by Ducci et al. to the observed X-ray light curve. Assuming an eccentricity of $e = 0.4$, the X-ray emission from this source can be explained in terms of the accretion from a spherically symmetric clumpy wind, composed of clumps with different masses, ranging from 10^{18} g to 5×10^{21} g.

Key words: X-rays: binaries – X-rays: individual: IGR J18483−0311.

1 INTRODUCTION

The X-ray transient IGR J18483−0311 was discovered during the observations of the Galactic plane with *INTEGRAL* in 2003 April (Chernyakova et al. 2003), when it reached a flux of 10 mCrab in the 15–40 keV energy range. Five more hard X-ray outbursts were reported by Sguera et al. (2007) with *INTEGRAL*, three of which exceeded one day in duration. The strongest outburst (∼1.8 d) occurred in 2006 April and reached a flux of 120 mCrab. The IGR J18483−0311 broad-band joint Joint European X-ray Monitor/Integral Soft Gamma-Ray Imager (JEM-X/ISGRI) *INTEGRAL* spectrum (3–50 keV) was fitted with an absorbed power law with a photon index, $\Gamma = 1.4 \pm 0.3$, a high absorption, $N_{\rm H} = 9^{+5}_{-4} \times 10^{22}$ cm^{-2} (higher than the Galactic at 1.4×10^{22} cm^{-2}) and a cut-off at ∼22 keV (Sguera et al. 2007).

A periodicity at 18.55 ± 0.03 d was discovered in the All-Sky Monitor/Rossi X-ray Timing Explorer (ASM/*RXTE*) light curves (Levine & Corbet 2006), and was interpreted as the orbital period of a binary system. Sguera et al. (2007) confirmed a similar period in the 20–40 keV ISGRI/*INTEGRAL* data (18.52 ± 0.01 d) and discovered pulsations at 21.0526 ± 0.0005 s with the X-ray monitor JEM-X. Skinner et al. (2008) refined the orbital period value to 18.518 ± 0.005 d, by using the much denser sampling provided by the *Swift*/Burst Alert Telescope (BAT) data.

From the observed values of the orbital and pulse periods, the position in the Corbet diagram (Corbet 1986) suggested at first a Be/X-ray transient nature (Sguera et al. 2007), but the optical and infrared observations of the X-ray error box estimated with *Swift* (Sguera et al. 2007) revealed that the donor star is a blue supergiant (B0.5Ia), and not a Be star, located at a distance of 3–4 kpc (Rahoui & Chaty 2008). The X-ray position was later refined with *Chandra* (Giunta et al. 2009), confirming this optical/infrared association. This implied the identification of this source as a new member of the class of the supergiant fast X-ray transients (SFXTs; Sguera et al. 2005, 2006; Negueruela et al. 2006; Sidoli 2009), although the dynamical range of its X-ray emission seems to be smaller than in other members of the same class. IGR J18483−0311 and IGR J11215−5952 are the only two SFXTs where both orbital and pulse periods have been discovered (Sidoli et al. 2006; Swank et al. 2007; Romano et al. 2009b).

⋆E-mail: romano@ifc.inaf.it

2 OBSERVATIONS AND DATA REDUCTION

The observations of IGR J18483−0311 were obtained as a target of opportunity (ToO) monitoring program with *Swift*. As shown in Table 1, the ToO observations started on 2009 June 11 with ∼2 ks per day. The campaign lasted 28 days divided into 23 observations for a total on-source exposure of ∼44 ks.

The X-ray Telescope (XRT) data were processed with standard procedures (XRTPIPELINE v0.12.1), filtering and screening criteria by using FTOOLS in the HEASOFT package (v.6.6.1). Both Windowed Timing (WT) and Photon Counting (PC) events were considered. The selection of event grades was 0–2 and 0–12 for WT and PC data, respectively (Burrows et al. 2005). We corrected for pile-up when required. The light curves were also corrected for point spread function (PSF) losses, vignetting and background-subtracted. Ancillary response files were generated with XRTMKARF to account for different extraction regions, vignetting and PSF corrections. We used the spectral redistribution matrices v011 in CALDB.

The Ultraviolet/Optical Telescope (UVOT) observed the target simultaneously with the XRT with the v filter (observations 004 through 006), and with the u filter (observations 007 though 010). For the remainder of the campaign, IGR J18483−0311 was observed with the 'filter of the day', i.e. the filter chosen for all observations to be carried out during a specific day in order to minimize the filter wheel usage (Roming et al. 2005). The data analysis was performed using the UVOTIMSUM and UVOTSOURCE tasks included in the FTOOLS. The latter task calculates the magnitude through aperture photometry within a circular region and applies specific corrections due to the detector characteristics. The reported magnitudes are on the UVOT photometric system described in Poole et al. (2008), and are not corrected for Galactic extinction. At the position of IGR J18483−0311, no detection was achieved down to a limit of $v > 21.07$ mag and $u > 21.19$ mag.

Table 1. Summary of the *Swift*/XRT observations.

Seq.	Start time (UT)	End time (UT)	Exp. (s)	Phase[a]
004	2009-06-11 14:42:17	2009-06-11 21:13:56	1606	0.07
005	2009-06-12 16:09:36	2009-06-12 19:34:56	1522	0.12
006	2009-06-13 18:08:11	2009-06-13 21:26:57	1774	0.18
007	2009-06-14 04:55:39	2009-06-14 08:20:57	1671	0.21
008	2009-06-15 10:03:12	2009-06-15 23:02:58	1977	0.28
009	2009-06-16 07:10:02	2009-06-16 12:08:58	1857	0.32
010	2009-06-17 00:42:44	2009-06-17 04:12:56	2047	0.36
012	2009-06-19 08:37:38	2009-06-19 12:02:56	2189	0.49
013	2009-06-20 13:32:09	2009-06-20 16:57:56	2291	0.55
016	2009-06-23 07:51:16	2009-06-23 12:53:56	2003	0.70
017	2009-06-24 09:32:31	2009-06-24 14:35:56	2711	0.76
018	2009-06-25 04:33:46	2009-06-25 12:52:56	1870	0.81
019	2009-06-26 15:43:27	2009-06-26 19:06:57	1884	0.88
020	2009-06-27 04:33:51	2009-06-27 07:56:57	1824	0.91
021	2009-06-28 03:16:17	2009-06-28 08:14:56	1922	0.96
022	2009-06-29 11:30:17	2009-06-29 11:47:57	1057	0.03
023	2009-06-30 06:47:17	2009-06-30 11:54:57	2616	0.08
024	2009-07-01 02:17:22	2009-07-01 12:00:57	2070	0.13
025	2009-07-02 10:22:32	2009-07-02 13:23:57	2408	0.19
026	2009-07-03 07:01:47	2009-07-03 10:31:58	2106	0.24
027	2009-07-04 07:05:17	2009-07-04 10:36:27	2560	0.29
029	2009-07-06 02:15:18	2009-07-06 08:53:58	1838	0.39
030	2009-07-08 07:32:02	2009-07-08 07:37:56	340	0.51

[a]Calculated according to Sguera et al. (2007).

All quoted uncertainties are given at 90 per cent confidence level for one interesting parameter unless otherwise stated. The spectral indices are parametrized as $F_\nu \propto \nu^{-\alpha}$, where F_ν (erg cm^{-2} s^{-1} Hz^{-1}) is the flux density as a function of frequency ν; we adopt $\Gamma = \alpha + 1$ as the photon index, $N(E) \propto E^{-\Gamma}$ (ph cm^{-2} s^{-1} keV^{-1}).

3 RESULTS

3.1 Light curve

Fig. 1 shows the 0.2–10 keV light curve of IGR J18483−0311 of the whole campaign after background-subtraction and pile-up, PSF losses, and vignetting corrections. Each bin contains a minimum of 20 source counts. The light curve starts at phase 0.07, assuming a period of 18.52 d and an initial epoch MJD 53844.2 (Sguera et al. 2007), and monitors the flux state through a whole period until the following phase 0.51. Superimposed on the long-term orbital modulation, variability is seen on short time-scales, as shown in the inset of Fig. 1, where a variation by factor of 5.3 in count rate is observed to occur in ∼1.7 h. This behaviour has been observed in several SFXTs (e.g. Sidoli et al. 2008; Romano et al. 2009a).

The lowest point in the campaign is a 3σ upper limit reached on MJD 55006.5–55010.2 at 0.004 counts s^{-1} (combined observations 017–020, total on-source exposure of 8.3 ks), and corresponds to an observed (unabsorbed) flux of 3.9×10^{-13} (2.1×10^{-12}) erg cm^{-2} s^{-1}, if we assume the *XMM–Newton* spectrum reported by Giunta et al. (2009, photon index $\Gamma = 2.5$, absorbing column $N_{\rm H} = 7.7 \times 10^{22}$ cm^{-2}). The corresponding luminosity is 2.3×10^{33} erg s^{-1} (assuming the optical counterpart distance of 3 kpc); to date, this is the lowest quiescent X-ray flux value reported in the literature for this source. The peak count rate is reached on MJD 55016.4 at $\gtrsim$5 counts s^{-1}; therefore, the observed dynamical range of this source is at least 1200.

In order to search for spin periodicity, the arrival times of all selected events have been converted to the Solar system barycentric frame, using the BARYCOR code. The Z^2 test (Buccheri et al. 1983) on the fundamental harmonics was applied to a sample of source photon arrival times for each observation. The search for a timing feature was performed within the frequency interval 0.01–0.19 s^{-1}. No presence of coherent pulsations was detected.

3.2 Spectra

Spectra were extracted for each segment in which a detection was obtained and a minimum of 120 source counts were available. The data were rebinned with at least 20 counts bin^{-1} to allow χ^2 fitting, except when the statistics were poor, in which case we adopted Cash (1979) statistics and data binned to 1 count bin^{-1}, instead. The simple models we considered were absorbed power laws and absorbed blackbodies. The fits were performed in the 0.3–10 keV energy band. The results are reported in Table 2, while the spectral parameters as a function of time are shown in Fig. 2. In particular, for the spectrum of observation 006, the highest in flux during the first peak ($\sim 1.5 \times 10^{-10}$ erg cm^{-2} s^{-1}), an absorbed power-law model yielded a high absorbing column $N_{\rm H} = (6.3^{+1.5}_{-1.2}) \times 10^{22}$ cm^{-2} and a photon index $\Gamma = 1.7 \pm 0.4$ (see Table 2). As a comparison, observation 025, roughly at the same phase, yielded $N_{\rm H} = (7.1^{+1.1}_{-1.0}) \times 10^{22}$ cm^{-2} and $\Gamma = 1.6 \pm 0.3$, hence consistent with observation 006. Despite the large observed variations in flux throughout the campaign, the spectral parameters do not vary significantly within the large uncertainties, with the exception of the blackbody radii.

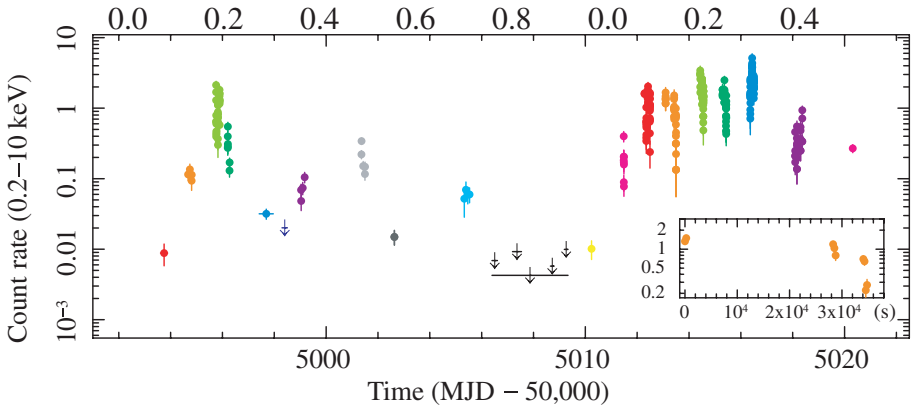

Figure 1. *Swift*/XRT 0.2–10 keV light curve of IGR J18483−0311 during our monitoring program, background-subtracted and corrected for pile-up, PSF losses and vignetting. Downward-pointing arrows are 3σ upper limits. The upper limit with the wide symbol centred on MJD 55007.9 ($\sim$0.004 counts s^{-1}) is obtained accumulating the four observations (individual upper limits) between MJD 55006.5 and 55010.2. Different colours mark different observations (see Table 1), with a colour scheme that generally mimics the phase (top axis) with a $P = 18.52$ d (Sguera et al. 2007). The inset zooms on observation 024.

Table 2. XRT spectroscopy.

Seq.	Power-law				Blackbody					
	$N_{\rm H}$ (10^{22} cm^{-2})	Γ	Flux[a] (2–10 keV)	$\chi^2_{\rm red}$/d.o.f. C-stat (per cent)[c]	$N_{\rm H}$ (10^{22} cm^{-2})	kT (keV)	$R_{\rm BB}$ (km)[d]	Flux[a] (2–10 keV)	L[b] (2–10 keV)	$\chi^2_{\rm red}$/d.o.f C-stat (per cent)[c]
005	$6.0^{+3.4}_{-2.5}$	$1.4^{+0.9}_{-0.8}$	$1.90^{+0.37}_{-0.94}$	102.1(48.3)	$3.5^{+2.2}_{-1.6}$	$1.6^{+0.6}_{-0.4}$	$0.14^{+0.03}_{-0.01}$	$1.46^{+0.15}_{-0.83}$	0.2	100.9(31.90)
006	$6.3^{+1.5}_{-1.2}$	$1.7^{+0.4}_{-0.4}$	$15.46^{+0.54}_{-3.45}$	1.1/34	$3.1^{+0.8}_{-0.7}$	$1.6^{+0.2}_{-0.2}$	$0.43^{+0.22}_{-0.14}$	$11.3^{+0.79}_{-1.99}$	1.2	1.1/34
007	$4.8^{+3.8}_{-2.1}$	$1.3^{+0.9}_{-0.7}$	$2.72^{+0.39}_{-0.92}$	1.2/9	$2.5^{+2.0}_{-1.2}$	$1.6^{+0.5}_{-0.3}$	$0.17^{+0.04}_{-0.02}$	$2.06^{+0.24}_{-0.99}$	0.2	0.9/9
010	$6.6^{+2.7}_{-2.2}$	$2.1^{+0.8}_{-0.7}$	$1.45^{+0.12}_{-0.68}$	119.0(27.2)	$3.5^{+1.7}_{-1.4}$	$1.3^{+0.3}_{-0.2}$	$0.18^{+0.05}_{-0.02}$	$1.00^{+0.10}_{-0.46}$	0.1	117.5(10.58)
012	$6.4^{+3.0}_{-2.1}$	$1.8^{+0.7}_{-0.6}$	$2.78^{+0.19}_{-1.05}$	1.2/13	$3.2^{+1.7}_{-1.2}$	$1.5^{+0.3}_{-0.2}$	$0.20^{+0.05}_{-0.02}$	$1.98^{+0.16}_{-0.71}$	0.2	1.1/13
022	$16.5^{+7.7}_{-6.1}$	$2.3^{+1.2}_{-1.1}$	$5.79^{+0.30}_{-4.33}$	97.43(26.7)	$10.7^{+5.2}_{-4.0}$	$1.5^{+0.6}_{-0.3}$	$0.27^{+0.28}_{-0.08}$	$3.43^{+0.22}_{-2.24}$	0.4	98.02(12.17)
023	$6.6^{+1.4}_{-1.2}$	$1.4^{+0.3}_{-0.3}$	$17.44^{+0.51}_{-3.38}$	0.9/51	$3.7^{+0.8}_{-0.7}$	$1.7^{+0.2}_{-0.2}$	$0.39^{+0.15}_{-0.10}$	$13.26^{+0.62}_{-2.14}$	1.4	1.0/51
024	$10.4^{+2.9}_{-2.3}$	$1.5^{+0.5}_{-0.4}$	$19.97^{+0.58}_{-6.79}$	0.7/25	$6.3^{+1.8}_{-1.4}$	$1.9^{+0.3}_{-0.3}$	$0.37^{+0.19}_{-0.11}$	$14.78^{+0.84}_{-4.13}$	1.6	0.7/25
025	$7.1^{+1.1}_{-1.0}$	$1.6^{+0.3}_{-0.3}$	$32.83^{+0.87}_{-4.92}$	1.1/71	$3.8^{+0.7}_{-0.6}$	$1.7^{+0.2}_{-0.1}$	$0.56^{+0.38}_{-0.27}$	$24.23^{+0.92}_{-3.19}$	2.6	1.2/71
026	$6.3^{+1.3}_{-1.1}$	$1.2^{+0.3}_{-0.3}$	$20.83^{+0.88}_{-3.87}$	1.0/42	$3.7^{+0.8}_{-0.7}$	$1.9^{+0.2}_{-0.2}$	$0.38^{+0.14}_{-0.09}$	$16.68^{+0.94}_{-3.08}$	1.8	1.0/42
027	$6.6^{+0.9}_{-0.8}$	$1.3^{+0.2}_{-0.2}$	$43.22^{+1.18}_{-5.46}$	0.8/81	$3.8^{+0.6}_{-0.5}$	$1.9^{+0.2}_{-0.1}$	$0.56^{+0.29}_{-0.22}$	$34.14^{+1.39}_{-3.64}$	3.7	0.8/81
029	$7.9^{+2.6}_{-1.9}$	$1.8^{+0.5}_{-0.5}$	$6.55^{+0.20}_{-2.17}$	1.4/25	$4.3^{+1.4}_{-1.1}$	$1.6^{+0.2}_{-0.2}$	$0.28^{+0.09}_{-0.05}$	$4.64^{+0.30}_{-1.18}$	0.5	1.3/25
High[e]	$5.4^{+0.5}_{-0.4}$	$1.0^{+0.1}_{-0.1}$	$25.77^{+0.46}_{-1.48}$	1.0/222	$3.2^{+0.3}_{-0.3}$	$2.1^{+0.1}_{-0.1}$	$0.37^{+0.05}_{-0.04}$	$21.25^{+0.56}_{-1.21}$	2.3	1.2/222
Medium[e]	$6.4^{+0.6}_{-0.5}$	$1.2^{+0.1}_{-0.1}$	$16.47^{+0.28}_{-1.06}$	1.0/212	$3.7^{+0.4}_{-0.3}$	$2.0^{+0.1}_{-0.1}$	$0.32^{+0.03}_{-0.03}$	$13.14^{+0.33}_{-0.69}$	1.4	1.1/212
Low[e]	$6.7^{+0.9}_{-0.8}$	$1.5^{+0.2}_{-0.2}$	$1.82^{+0.16}_{-0.06}$	1.0/115	$3.6^{+0.5}_{-0.5}$	$1.7^{+0.1}_{-0.1}$	$0.130^{+0.003}_{-0.002}$	$1.38^{+0.04}_{-0.11}$	0.2	0.8/115

[a]Fluxes (corrected for the absorption) are in units of 10^{-11} erg cm^{-2} s^{-1}.
[b]Luminosities in units of 10^{35} erg s^{-1}, assuming a distance of 3 kpc.
[c]Cash statistics (C-stat) and percentage of 10^4 Monte Carlo realizations that had statistics < C-stat.
[d]Blackbody radii are in units of km, assuming the optical counterpart distance of 3 kpc.
[e]Intensity-selected spectra. High corresponds to $CR > 1$ counts s^{-1}, medium to $0.5 < CR < 1$ counts s^{-1} and low to $CR < 0.5$ counts s^{-1}.

To further investigate the spectral properties of the sources in several states, we accumulated all events collected during the current campaign. We extracted events within three intensity levels depending on count rate, namely, CR $>$ 1 counts s^{-1} (high, 5447 counts), 0.5 $<$ CR $<$ 1 counts s^{-1} (medium, 5264 counts) and CR $<$ 0.5 counts s^{-1} (low, 2670 counts). We created exposure maps for each of these intensity-selected event files and then combined them (and their exposure maps), and extracted a single spectrum for each state. The generation of ancillary response files and spectral fitting were performed in the same fashion as for the single observation. The fit results are reported in Table 2 and the spectra are shown in Fig. 3. Even with the higher statistics afforded by accumulating all events in three intensity states, no significant variations in the column density could be derived. We can confirm, however, that the $N_{\rm H}$ is always in excess of the Galactic one, 1.4×10^{22} cm^{-2}, consistently with that found by Sguera et al. (2007). Similarly to what was found in a sample of four SFXTs (Romano et al. 2009a), our fits indicate either a hard power law or hot blackbody. We also note that all spectral fits with an absorbed blackbody resulted in radii of the emitting blackbody region of only a few hundred meters (see Table 2), consistent with being emitted from a small portion of the neutron star surface, such as its polar caps (see Romano et al. 2009a).

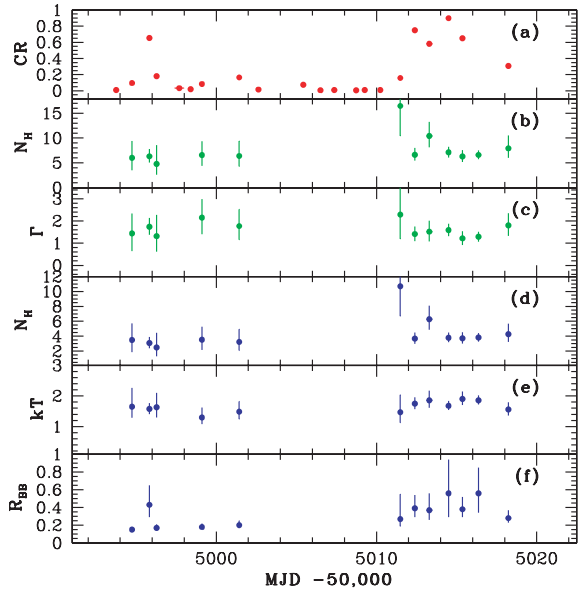

Figure 2. Spectral parameters as a function of time (see Table 2). (a) *Swift*/XRT light curve in the 0.2–10 keV energy band at a day resolution; spectral parameters of the absorbed power-law fit, $N_{\rm H}$, and photon index Γ [(b) and (c)]; spectral parameters of the absorbed blackbody fit, $N_{\rm H}$, temperature kT and blackbody radius [(d), (e), and (f)].

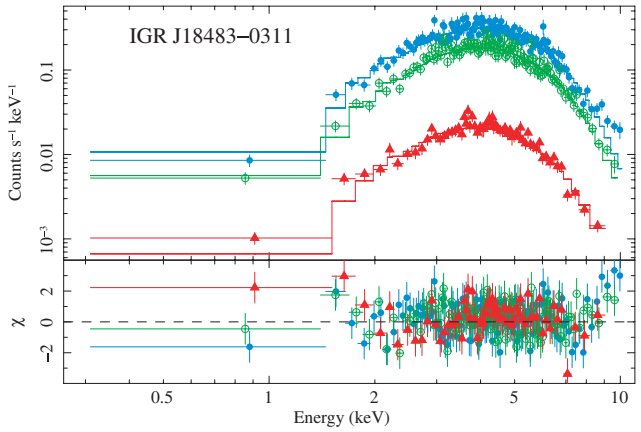

Figure 3. Intensity-selected spectroscopy. Upper panel: *Swift*/XRT data fit with an absorbed power law. Lower panel: the residuals of the fit (in units of standard deviations). Filled blue circles, green empty circles and red filled triangles mark high, medium and low state, respectively.

4 DISCUSSION

In this paper, we report on the first complete monitoring of the X-ray activity along an entire orbital period of a SFXT. This makes these *Swift* observations a unique data set, which allows us to constrain the different mechanisms proposed to explain the nature of this new class of X-ray transients. IGR J18483−0311 and IGR J11215−5952 are the only SFXTs where both the orbital and spin periods are known, although the two systems are very different ($P_{\rm orb} \sim 165$ d, $P_{\rm spin} \sim 190$ s in IGR J11215−5952; see, e.g. Romano et al. 2009b).

The *Swift* light curve appears to be highly modulated, with two maxima, separated by a time interval consistent with the orbital period of ∼18.5 d. A lower limit of 1200 to the dynamical range can be obtained from the observed light curve. The different duration of the two outburst peaks monitored with *Swift* is probably the result of both a different sampling and a high intrinsic X-ray variability. The second peak has a duration of several days, as previously observed by *INTEGRAL* (Sguera et al. 2007).

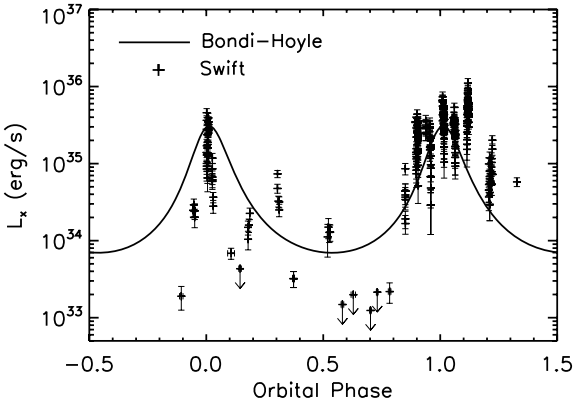

Figure 4. Comparison of the *Swift*/XRT light curve of IGR J18483−0311 (crosses) with the prediction of Bondi–Hoyle accretion from a spherically symmetric and homogeneous wind. We assumed a distance of 3 kpc. The model-dependent orbital phase $\phi = 0$ corresponds to 54995.83 MJD.

The modulation of the overall shape of the light curve with the orbital phase can be interpreted as wind accretion along a highly eccentric orbit. Thus, we applied different models for the wind accretion to gain information on the source parameters.

The simplest case is a Bondi–Hoyle accretion from a spherically symmetric and homogeneous wind. Assuming a supergiant mass of $M_{\rm OB} = 33\,{\rm M}_{\odot}$ and a radius, $R_{\rm OB} = 33.8\,{\rm R}_{\odot}$ (Searle et al. 2008), together with the known orbital period of $P_{\rm orb} = 18.52$ d, we tried to account for the overall shape of the X-ray light curve, leaving the orbital eccentricity e as a free parameter. We assumed the following values for the wind properties: a terminal velocity v_{∞} in the range 1400–1800 km s^{-1}, a mass loss rate $\dot{M}$ in the range 0.4–1.5 $\times$ $10^{-6}\,{\rm M}_{\odot}\,{\rm yr}^{-1}$ (see Lefever et al. 2007; Searle et al. 2008). In this framework, we obtain the best agreement with the observed light curve by assuming an eccentricity $e = 0.4$, $v_{\infty} = 1800$ km s^{-1}, $\dot{M} = 5 \times 10^{-7}\,{\rm M}_{\odot}\,{\rm yr}^{-1}$, $\beta = 1$. Fig. 4 shows the comparison of the model predictions and the observed *Swift*/XRT light curve (in units of erg s^{-1}, by assuming a distance of 3 kpc). The model roughly reproduces the shape of the X-ray light curve due to the orbital modulation, with the largest deviation from the observations being in the time interval MJD 55006.5−55010.2, where we observed four upper limits. Note, however, that we cannot be sure that the low intensity extends for four days continuously, because the four *Swift* observations consist of short snapshots. We investigated the possibility that these upper limits could be due to the onset of a centrifugal inhibition for the accretion (Davidson & Ostriker 1973). For the above adopted set of wind and orbital parameters, we calculated a new X-ray light curve, finding that a low magnetic field of the neutron star of $B \approx 4 \times 10^{11}$ G could be responsible for the upper limits at MJD 55006.5−55010.2 (see Fig. 5).

An alternative scenario to explain the low intensity state is an X-ray eclipse of the neutron star by the supergiant companion. Assuming a circular orbit, we obtain a lower limit to the radius of the supergiant star (Rappaport & Joss 1983) of $R_{\rm OB} = 46\,{\rm R}_{\odot}$, which is too large for a B0.5a supergiant (Searle et al. 2008). On the other hand, our modelling of the X-ray curve suggests a high eccentricity of at least $e = 0.4$. Adopting this eccentricity, we derived an expected value for the supergiant radius of $R_{\rm OB} = 39.5\,{\rm R}_{\odot}$. The radii of B0.5Ia stars are usually smaller than this value, but there are several exceptions with $R \approx 40\,{\rm R}_{\odot}$ (Lefever et al. 2007; Searle et al.

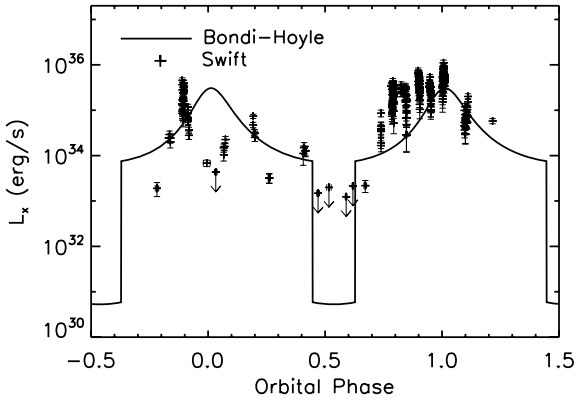

Figure 5. Comparison of the *Swift*/XRT light curve of IGR J18483−0311 (crosses) with the prediction of Bondi–Hoyle accretion from a spherically symmetric and homogeneous wind, assuming a magnetic field $B = 4 \times 10^{11}$ G. The model-dependent orbital phase $\phi = 0$ corresponds to 54997.69 MJD.

2008). Therefore, we cannot exclude that an eclipse is responsible for the low luminosity state in an eccentric orbit.

Although both centrifugal inhibition and an eclipse can reconcile the observed low intensity state with the Bondi–Hoyle accretion predictions, it is also clear that the spherically symmetric and homogeneous wind only reproduces the overall shape of the X-ray light curve. It cannot, indeed, account for the very large spread around the average behaviour due to the orbital modulation and, most of all, the remarkable short time-scale variability (see, for example, the inset in Fig. 1, where a variation by a factor of 5.3 in count rate is observed in ∼1.7 h). The observed short time-scale variability can be naturally explained by the accretion of single clumps composing the donor wind. Thus, in order to improve the agreement between the observed and the calculated light curve, we applied the isotropic clumpy wind model proposed by Ducci et al. (2009).

The Ducci et al. (2009) model was developed to investigate the effects of accretion from a clumpy wind on the luminosity and variability properties of high-mass X-ray binaries. It assumes that a fraction of the stellar wind is in the form of clumps with a power-law mass distribution

$$p(M_{\rm cl}) = k \left(\frac{M_{\rm cl}}{M_{\rm a}}\right)^{-\zeta} \quad (1)$$

in the mass range $M_{\rm a} - M_{\rm b}$. The rate of clumps produced by the supergiant is related to the total mass loss rate $\dot{M}_{\rm tot}$ by $\dot{N}_{\rm cl} = f\dot{M}_{\rm tot}/\langle M\rangle$ clumps s^{-1}, where $f = \dot{M}_{\rm cl}/\dot{M}_{\rm tot}$ is the fraction of mass lost in clumps and $\langle M\rangle$ is the average clump mass, which can be computed from equation (1). Clumps are driven radially outward by absorption of UV spectral lines. The following clump velocity profile is assumed: $v_{\rm cl}(r) = v_\infty\left(1 - 0.9983\frac{R_{\rm OB}}{r}\right)^\beta$, where v_∞ is the terminal wind velocity, $R_{\rm OB}$ is the radius of the supergiant, 0.9983 is a parameter which ensures that $v(R_{\rm OB}) \approx 10$ km s^{-1} and β is a constant in the range ∼0.5–1.5. The model further assumes that the clumps are confined by ram pressure of the ambient gas. By exploring different distributions for the clump masses and initial dimensions, the model can be used to compute the expected X-ray light curves in the framework of the Bondi–Hoyle accretion theory, modified to take into account the presence of clumps. We sought the set of wind parameters yielding the best agreement between the calculated and the observed light curve. We found that the observed light curve is reproduced well by this wind model by assuming the following parameter values: an eccentricity $e = 0.4$, a

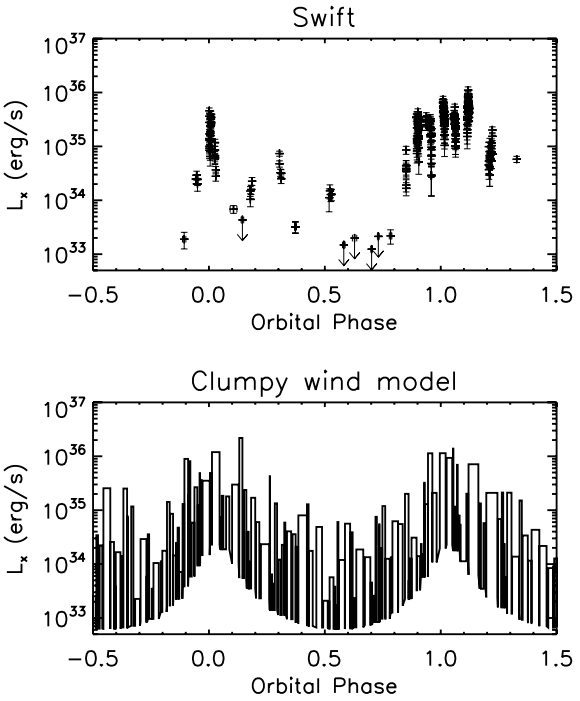

Figure 6. Comparison of the *Swift*/XRT light curve of IGR J18483−0311 (top) with the prediction (bottom) of the new clumpy wind model of Ducci et al. (2009). The model-dependent orbital phase $\phi = 0$ corresponds to 54995.83 MJD.

mass loss rate $\dot{M}_{\rm tot} = 2 \times 10^{-7}\,{\rm M}_\odot\,{\rm yr}^{-1}$, $v_\infty = 1800$ km s^{-1}, $\beta = 1$, a fraction of mass lost in clumps $f = 0.75$, a mass distribution power-law index $\zeta = 1.1$, a power-law index of the initial clump dimension distribution $\gamma = -1$ (where $\dot{N}_{M_{cl}} \propto R_{\rm cl}^\gamma$ clumps s^{-1}), a minimum clump mass $M_{\rm a} = 10^{18}$ g and a maximum clump mass $M_{\rm b} = 5 \times 10^{21}$ g; moreover, we adopt the force multiplier parameter obtained by Shimada et al. (1994) for a B0.5Ia star ($k = 0.375$, $\alpha = 0.522, \delta = 0.099$).

Fig. 6 shows the comparison of the *Swift*/XRT light curve of IGR J18483−0311 with the isotropic clumpy wind model prediction. Further acceptable solutions can be found by assuming wind parameters ζ, f, γ in the allowed ranges plotted in Fig. 7, and $e = 0.4 \pm 0.1$, $\dot{M}_{\rm tot} = (2 \pm 1) \times 10^{-7}\,{\rm M}_\odot\,{\rm yr}^{-1}$, $v_\infty = 1800$ km s^{-1}, $\beta = 1$, $10^{18} \le M_{cl} \le 10^{21}$ g. As Fig. 7 demonstrates, the comparison of the observed light curve with the clumpy wind model allowed us to constrain the parameters responsible for the degree of inhomogeneity of the wind. In particular, we found that a very large fraction of the mass lost from the supergiant is contained in the clumps ($0.7 \lesssim f \lesssim 0.78$), and we obtain the value of ζ (which controls the shape of the clump formation rate distribution) with an accuracy of ∼15 per cent.

Fig. 6 shows that the peak luminosities, the dynamic range involved by the flares, and the orbital modulation and the low luminosity state (MJD 55006.5−55010.2) observed are reproduced well by the clumpy wind model, even without invoking either a centrifugal barrier or an X-ray eclipse. Indeed, from the calculated light curve, we determined that the probability to observe the source at the interclump luminosity level in the range of phase $0.2 < \phi < 0.8$ is ∼25 per cent: with the binomial distribution function, we obtain a probability to measure four low luminosity states of ∼5 per cent. Therefore, the upper limits can be explained with the accretion of the intraclump wind with a low density, even without invoking

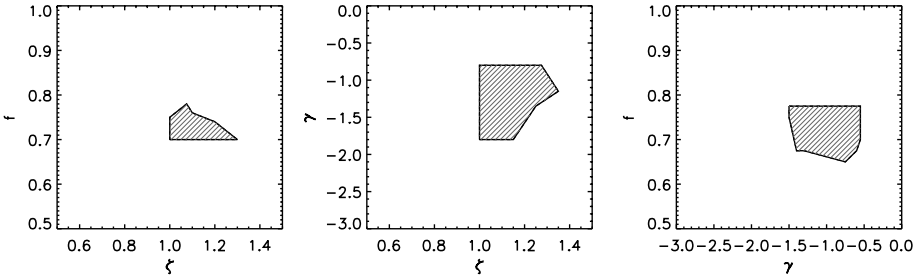

Figure 7. Graphs of the allowed parameters ζ, f, γ (filled region), obtained from the comparison between the observed and the calculated light curves.

centrifugal inhibition or an eclipse. Finally, we note that the wind parameters we obtain applying our spherical clumpy wind model (Ducci et al. 2009) are very similar to those explaining the Vela X–1 X-ray light curve. Indeed, the two systems have very similar donor stars.

ACKNOWLEDGMENTS

We thank the *Swift* team duty scientists and science planners. We also thank the remainder of the *Swift* XRT and BAT teams, S. Barthelmy and J. A. Nousek, in particular, for their invaluable help and support. This work was supported in Italy by contracts ASI I/088/06/0 and I/023/05/0, at PSU by NASA contract NAS5-00136. We thank P.A. Evans and S. Vercellone for helpful discussions. We also thank the anonymous referee for comments that helped improve the paper.

REFERENCES

Buccheri R. et al., 1983, A&A, 128, 245
Burrows D. N. et al., 2005, Space Sci. Rev., 120, 165
Cash W., 1979, ApJ, 228, 939
Chernyakova M., Lutovinov A., Capitanio F., Lund N., Gehrels N., 2003, Astron. Tel., 157
Corbet R. H. D., 1986, MNRAS, 220, 1047
Davidson K., Ostriker J. P., 1973, ApJ, 179, 585
Ducci L., Sidoli L., Mereghetti S., Paizis A., Romano P., 2009, MNRAS, 398, 2152
Giunta A., 2009, MNRAS, 399, 744
Lefever K., Puls J., Aerts C., 2007, A&A, 463, 1093
Levine A. M., Corbet R., 2006, Astron. Tel., 940
Negueruela I., Smith D. M., Reig P., Chaty S., Torrejón J. M., 2006, in Wilson A., ed., Proc. The X-ray Universe 2005, ESA SP-604, Volume 1. ESA, Noordwijk, 165
Poole T. S. et al., 2008, MNRAS, 383, 627
Rahoui F., Chaty S., 2008, A&A, 492, 163
Rappaport S. A., Joss P. C., 1983, in Lewin W. H. G., van den Heuvel E. P. J., eds, Accretion-Driven Stellar X-ray Sources. Cambridge Univ. Press, Cambridge, p. 1
Romano P. et al., 2009a, MNRAS, 399, 2021
Romano P., Sidoli L., Cusumano G., Vercellone S., Mangano V., Krimm H. A., 2009b, ApJ, 696, 2068
Roming P. W. A. et al., 2005, Space Sci. Rev., 120, 95
Searle S. C., Prinja R. K., Massa D., Ryans R., 2008, A&A, 481, 777
Sguera V. et al., 2005, A&A, 444, 221
Sguera V. et al., 2006, ApJ, 646, 452
Sguera V. et al., 2007, A&A, 467, 249
Shimada M. R., Ito M., Hirata B., Horaguchi T., 1994, in Balona L. A., Henrichs H. F., Le Contel J. M., eds, Proc. IAU Symp., Vol. 162, Pulsation; Rotation; and Mass Loss in Early-Type Stars. Kluwer, Dordrecht, p. 487
Skinner G., Tueller J., Beckmann V., Corbet R., Farrell S., Krimm H. A., Markwardt C., 2008, Proc. 7th INTEGRAL Workshop
Sidoli L., 2009, Advances Space Res., 43, 1464
Sidoli L., Paizis A., Mereghetti S., 2006, A&A, 450, L9
Sidoli L. et al., 2008, ApJ, 687, 1230
Swank J. H., Smith D. M., Markwardt C. B., 2007, ATel, 999

This paper has been typeset from a TEX/LATEX file prepared by the author.